# On Modelling Geophysical Flows Having Low Rossby Numbers

David E. Dietrich[1]
*Ecodynamics Research Associates, Inc.*
*P.O. Box 9229, Albuquerque*
*New Mexico 87119 U.S.A.*
*and*
*Visiting Scientist, Department of Atmospheric and Oceanic Sciences*
*McGill University, Montréal, Quebec*

[Original manuscript received 3 August 1990; in revised form 14 August 1991]

ABSTRACT *New, fourth-order "c" grid Coriolis term treatments are compared with widely used second-order treatments. Their improved accuracy is demonstrated by a grid convergence study for a relevant linear problem. Such an accuracy improvement is relatively easy and costs little for low Rossby number flows compared with high Rossby number flows, because one must consider only the Coriolis and pressure gradient terms in low Rossby number flows. The "c" grid is favourable for the latter, but the Coriolis terms benefit greatly by the higher order treatments analysed herein.*

RÉSUMÉ *On compare les applications d'un nouveau terme de quatrième ordre de Coriolis de la grille « c » aux applications de deuxième ordre grandement utilisées. On démontre leur meilleure précision par une étude de convergence de grille pour un problème linéaire donné. Une telle amélioration de la précision est relativement facile et coûte peu pour des flux de petit nombre de Rossby comparée aux flux de grand nombre car, avec le petit nombre, on ne doit considéré que les termes de Coriolis et de gradient de pression. La grille « c » est favorable à cette dernière, mais les termes de Coriolis profitent grandement des applications de plus grand ordre analysées.*

## 1 Introduction

Geophysical flows are generally strongly rotating. The Coriolis terms are much larger than the advection terms in the earth's rotating frame for the major flow components, especially for ocean flows. Thus, rather than focusing on the accuracy of the advection terms, as is often done, we are more interested in the accuracy of the dominant Coriolis, pressure gradient and horizontal divergence terms.

Spectral and other Galerkin-like methods often handle these dominant linear

[1]Present affiliation: Center for Air Sea Technology, Mississippi State University, Stennis Space Center, Mississippi 39529-6000 U.S.A.

*ATMOSPHERE-OCEAN 31* (1) 1993, 57–71 0705-5900/93/0000-0057$01.25/0

terms analytically in the time-differenced equations, which gives them a huge advantage – at the expense of increased computations for the non-linear advection terms. They are much less efficient if applied with proper lateral boundary conditions in complex ocean geometries. Thus, Galerkin-like methods might be better suited for representing relatively simple vertical structures, especially in the ocean, than for horizontal structures. Such an approach has been used successfully in tidal modelling (Davies and Furnes, 1980). Although vertical variance might be dominated by a few modes, thermocline dynamics might be difficult to address accurately, because vertical derivatives of frontal-like structures are involved, unless time and laterally dependent characteristic Galerkin functions are used. Methods to automate time-dependent basis functions exist, such as described by Dietrich (1972). An analogous finite-difference approach would be to use a time and laterally dependent vertical grid. Such a grid would be bottom boundary-fit, with no extra complication.

Thus, although the optimum vertical representation is not clear, finite-difference methods appear better suited than spectral methods for horizontal representation in the oceans. More general finite-element methods (Perkins, pers. commun., 1992), that can be accurately fit to complicated boundaries are also of interest and are being developed for ocean modelling.

The focus here is to analyse improved horizontal grid methods introduced by Dietrich et al. (1990), hereafter DRM, in modelling the dominant linear terms. In particular, we focus on the representation of the Coriolis terms on the staggered Arakawa "c" grid (Arakawa and Lamb, 1981).

The Coriolis terms dominate the acceleration terms in ocean flows nearly everywhere, as indicated by the smallness of the Rossby number. For typical ocean eddies of 200-km width and velocity 10 cm $s^{-1}$, the Rossby number is O(0.01). Thus, accurate modelling of ocean flows for low Rossby numbers requires accurate integration of the Coriolis terms.

Although boundary currents often have smaller scales and larger Rossby numbers, their Rossby numbers are still usually quite small. Further, the conventional Rossby number, based on boundary current width, overestimates the effective ratio of the advection term to the Coriolis term when the velocity is nearly normal to the local velocity gradients, which often occurs with boundary currents. (The advection is exactly zero when the gradient is normal to the velocity, yet the usual Rossby number scaling gives a misleading finite value.) In assessing the magnitude of the advection terms relative to the Coriolis terms, which is the relevant ratio here, the appropriate length scale is the distance *along the flow direction* over which order unity variations typically occur – i.e. over which the velocity changes are comparable with the velocity. This is generally much larger than the width of the boundary current. (Indeed, this is what characterizes boundary currents.) Of course, the accuracy of the Coriolis terms helps overall accuracy even when they are less dominant.

Such Coriolis term accuracy is automatically satisfied by the Arakawa "b" staggered grid of the popular Bryan-Cox ocean model (Bryan and Cox, 1968; Cox,

1984), especially with the small time step normally used with high resolution. The reason is that the horizontal velocity components are collocated, so that no interpolations are needed to evaluate the Coriolis terms.

Unlike the "b" grid, the Arakawa "c" staggered grid, which is much more widely used in general computational fluid dynamics, has spatial truncation errors in these terms, because of the interpolations needed to evaluate them. When the Coriolis terms are large, such truncation errors can dominate the total numerical error, even when the popular energy-conserving Arakawa scheme is used. Although such conservation is desirable, it has little to do with accuracy, which is the focus here.

To illustrate the physical impact of such errors, consider an initial value problem in which all terms other than the Coriolis and local time derivatives are neglected. If the initial velocity is zero everywhere except at one point, the analytic solution has zero velocity everywhere except at that point for all time. However, the spatial averaging required to evaluate the Coriolis terms on the "c" grid necessarily leads to non-zero values everywhere. Energy is thus dispersed erroneously. Such numerical dispersion reflects the truncation error that occurs in the interpolations needed to evaluate the Coriolis terms on the "c" grid.

However, the "c" grid is popular in spite of the performance of its Coriolis terms, because accurate modelling of geophysical flows also requires accurate treatment of the pressure gradient and horizontal divergence terms, which are important internal wave terms. (Vertical velocity divergence and vertical density advection are also involved, but have no bearing on the choice of the horizontal "b" or "c" grid.) The "c" grid is more accurate for these terms, because the data that are used for their centred first derivative finite-difference approximations are more closely spaced than on the "b" grid. This advantage also applies to higher order approximations.

Thus, for typical low Rossby number geophysical flows, the relative accuracy of the "b" and "c" grids depends mainly on whether the Coriolis or internal wave terms dominate. The internal Rossby radius of deformation – the distance an internal wave travels in one inertial (Coriolis) period – is a scale for which these two effects (buoyancy and rotation) typically contribute about the same to the local time derivative. Smaller scales are dominated by the internal wave terms; larger scales are dominated by the Coriolis terms. Thus, if the largest "b" grid errors occur for scales of the same order or smaller than the Rossby radius of deformation, and these scales are resolved by the calculation, the use of a "c" grid usually leads to smaller errors with the same resolution. Further discussion of the relative merits of the "b" and "c" grids is given by Messinger and Arakawa (1976), Bateen and Han (1981), Wajsowicz (1986a, b), Wajsowicz and Gill (1986) and Foreman (1987).

Since the dominant ocean eddy and boundary current scales are comparable with the Rossby radius of deformation, it follows that the preferred grid for ocean eddy-resolving calculations is the "c" grid. Notably, the effect of these eddies on the ocean large-scale circulation has not yet been addressed adequately by turbulence closure schemes.

Since the "c" grid's main weakness stems from the interpolations required to evaluate the Coriolis terms, one is led to try using higher order interpolations for

this purpose when the flow has a low Rossby number. This, and the relatively modest computing overhead required, led to the development of new ocean models based on the Sandia Ocean Modeling System (SOMS) (Dietrich et al., 1987).

Here, we compare the popular standard Arakawa "c" grid Coriolis scheme with the original SOMS Coriolis scheme and the new higher-order version.

## 2 Background

The original SOMS "c" grid scheme for the Coriolis terms is described by Dietrich et al. (1987), and in Appendix 1. This scheme differs from the popular Arakawa "c" grid schemes and is characterized by its integration of the Coriolis terms at the pressure cell centres, while using the Arakawa "c" grid as the primary grid for momentum conservation. This design was motivated by the need for accurate, efficient boundary-layer modelling.

SOMS is a fully conservative, partially implicit ocean and lake modelling system, using a fully Eulerian frame with a "c" grid. It uses a separate boundary-fitted, three-dimensional boundary-layer submodel, which includes a Mellor-Yamada level 2.5 turbulence closure scheme (Mellor and Yamada, 1982). The boundary-layer submodel is coupled to an overlying free-stream submodel by pressure gradient and flux matching at their interface. The interface is a prescribed distance from the modelled basin bottom, such that the boundary-layer submodel contains the turbulent bottom boundary layer. This approach is motivated by boundary-layer theory, and is designed for bottom boundary phenomena over general topography.

SOMS started as a bottom ocean model, designed to interface between an eddy-resolving regional ocean model and the ocean bottom, in studying material dispersion from the ocean bottom (funded by the DOE Subseabed Waste Disposal Program). This application required accurate resolution of ocean eddies, which clearly can affect vertical mixing and possibly influence boundary-layer separation. This was a primary consideration in the decision to use an Arakawa "c" grid, which is best for eddy-resolving calculations, as explained above.

New, low (scheme 2A) and higher order Coriolis term treatments were introduced to SOMS by DRM. The SOMS schemes (four in all) require interpolation between the staggered "c" grid velocity locations and the pressure cell centres. The new higher-order versions (schemes 1B and 2B) differ from the corresponding lower order ones (schemes 1A and 2A) only by using higher order interpolations.

All four schemes described by DRM, and further analysed here, first partially update the velocity components at their staggered "c" grid locations. These partial updates include the effects of all terms except the Coriolis and vertical diffusion terms (i.e. the partial updates give temporary new values that would result from assuming these terms are zero). Any desired explicit time integration scheme can be used for the terms (advection, horizontal diffusion, and pressure gradient) included in these partial updates.

The time differences (from the partial updates) are then interpolated to the cell-centred pressure locations and treated as known explicit "source terms" for the remaining implicitly coupled Coriolis and vertical diffusion terms, which are then

solved implicitly at each pressure location. This gives the fully updated velocity at the pressure locations.

Schemes 1A and 1B then simply interpolate the updated velocity back to the staggered "c" grid. Schemes 2A and 2B replace this step with two steps:

1) The time-difference contributions due to the Coriolis and vertical diffusion terms at the pressure cell centres are separated from the other contributions.
2) These partial time-difference contributions are interpolated back to the staggered "c" grid and added to the original partially updated velocities at the "c" grid locations.

The final step is identical for all four schemes. This step is to "clear out the divergence" by appropriately modifying the top layer pressure, followed by adding the velocity response to this modification, as described by Dietrich et al. (1987).

More detailed descriptions of these schemes are given by DRM and in Appendix 1. DRM also describes a promising new "semi-collocated" scheme.

No special problems occur in using the new schemes with variable depth. Variable depth versions similar to the ones analysed by Foreman (1987) should be useful for continental shelf problems. The new schemes were applied to Lake Neuchatel (Zuur and Dietrich, 1990) with 263-m resolution and real topography. The results were in good agreement with observations. Recent results in Gulf of Mexico simulations with real (NCAR data) topography (Dietrich and Lin, 1993; Dietrich and Ko, 1993) also show good agreement with observations.

To analyse the new schemes, one can apply them to the full non-linear primitive equations in a prototype problem. For such systems, analytic solutions usually are not available, but one can compare them with observations and other model results, or carry out a grid convergence study, as DRM has done.

One can also apply the new schemes to relevant linear problems, which have analytic solutions, but there is the danger of simplifying too much. For example, one could include only the Coriolis and local time derivative terms, and study how well the schemes model inertial oscillations. However, such oscillations have little relevance in general circulation modelling, because pure inertial oscillations (and inertia-gravity waves) have little effect on net displacement during general circulation time-scales. Such oscillations might be more important in the atmosphere, because of their possible interaction with large-scale precipitation, as noted by Dietrich and Brunet (1979).

For relevance to general circulation modelling, the pressure-gradient terms must also be included. This gives the "maximum simplification problem" for relevant comparison. Here, we address this problem in a grid convergence study with specified characteristic analytic pressure fields. Errors (rms deviations from exact solutions to the pressure-forced flow) are then used to compare the new schemes with their lower order versions and with the constant-depth version of the widely used Arakawa "c" grid scheme.

Although this maximum simplification problem does not include internal wave dispersion terms, their primary role is to affect geostrophic adjustment. To obtain

a numerical geostrophic adjustment in the absence of these terms, we use a weak time damping (except as noted), which selectively filters high-frequency inertial oscillations. This damping is chosen such that it has little effect on longer time-scales relevant to general circulation calculations. This is a reasonable first step, since it is well known that the Arakawa "c" grid is ideal for the internal wave terms, but not as good for the Coriolis terms. The motivation of our new schemes is to improve modelling of the Coriolis terms on the "c" grid.

DRM showed that the new, higher-order Coriolis "c" grid schemes greatly improve accuracy in modelling the dominant ocean eddy scales in a prototype ocean problem. Here, we demonstrate this more conclusively, because

a) the present study focuses on the Coriolis terms, whereas DRM included other terms that, although small except near boundaries, were only second-order-accurate
b) the present fourth-order-accurate results have fourth-order-accuracy everywhere, whereas the Coriolis terms in the DRM study were only second-order-accurate near the boundary, which was acceptable because the other terms are relatively large and second-order-accurate there
c) we include direct comparison with the standard "c" grid Coriolis treatment

For the "b" grid and collocated (non-staggered) grids, analogous higher order treatment of the pressure gradient and divergence terms would probably lead to similar improvements.

The present improvement (b) required a minor adjustment of the interpolation coefficients used nearest the boundary. This improvement is to use a non-centred fourth-order interpolation scheme, rather than the boundary symmetry conditions applied in DRM. For example, the new approximation used to interpolate the $u$-velocity to the pressure point nearest a western boundary point (one-half grid interval from the boundary) is

$$u(0.5dx) = c_0 u(0) + c_1 u(dx) + c_2 u(2dx) + c_3 u(3dx)$$

where $u(0)$ is a specified boundary value (or function of $u(dx)$) and $u(dx)$, $u(2dx)$ and $u(3dx)$ are known interior values. The coefficients $c_0$, $c_1$, $c_2$ and $c_3$ are determined simply by fitting a cubic polynomial through the four known values, and evaluating the result at $x = 0.5dx$. This defines a general, unique scheme. There is nothing special about irregular (staircase) boundaries. The scheme is fourth-order accurate in general, as reflected by the fourth-order convergence behaviour in Table 1. The results in Section 3 show that the scheme is also robust. We are presently using it in multi-decade ocean-basin-scale calculations.

In spite of the boundary accuracy problem mentioned above, DRM showed a dramatic improvement in accuracy: the improved methods were as accurate with 20-km resolution as the more conventional methods were with 10-km resolution, with only a few per cent extra computation required per grid point. DRM shows this in many ways. One is the grid-resolution dependence of the peak rms velocity, resulting from baroclinic instability. For 40-, 20- and 10-km resolutions, respec-

TABLE 1. Normalized rms errors: the time-averaged rms velocity deviations from the exact solutions of the problem described in Section 3. The "base" scheme errors are calculated after interpolation of its staggered "c" grid velocities to the pressure locations.

| Scheme | Time Step (min) | Grid Size 12 × 12 | 24 × 24 | 48 × 48 |
|---|---|---|---|---|
| Base | 90 | $1.0 \times 10^{-1}$ | $2.9 \times 10^{-2}$ | $7.7 \times 10^{-3}$ |
| 1A | 90 | $1.0 \times 10^{-1}$ | $3.9 \times 10^{-2}$ | $1.3 \times 10^{-2}$ |
| 2A | 90 | $7.1 \times 10^{-2}$ | $2.5 \times 10^{-2}$ | $7.2 \times 10^{-3}$ |
| 1B | 180 | $1.7 \times 10^{-3}$ | $1.1 \times 10^{-4}$ | $6.6 \times 10^{-6}$ |
| | 90 | $4.1 \times 10^{-3}$ | $2.7 \times 10^{-4}$ | $1.7 \times 10^{-5}$ |
| | 45 | $1.2 \times 10^{-2}$ | $9.6 \times 10^{-4}$ | $6.5 \times 10^{-5}$ |
| 2B | 180 | $5.9 \times 10^{-4}$ | $3.8 \times 10^{-5}$ | $2.4 \times 10^{-6}$ |
| | 90 | $1.3 \times 10^{-3}$ | $8.6 \times 10^{-5}$ | $5.6 \times 10^{-6}$ |
| | 45 | $3.1 \times 10^{-3}$ | $2.1 \times 10^{-4}$ | $1.4 \times 10^{-5}$ |

tively, the peak rms velocities were 10.5, 15.2 and 18.3 cm $s^{-1}$ for the original scheme 1A. For the improved scheme 1B, they were 15.0, 19.2 and 20.9 cm $s^{-1}$. Thus, the change in scheme 1B from 20- to 10-km resolution is much smaller than the change from 40 to 20 km. A reasonable estimate of the converged value would be about 22 cm $s^{-1}$. Scheme 1B is closer to this estimated converged value with 20-km resolution than scheme 1A is with 10-km resolution.

## 3 Comparison of the new schemes and the standard "c" grid scheme

DRM noted that the interpolations used by the new "c" grid Coriolis scheme 1A lead to truncation errors $O((\Delta x)^2/\Delta t)$. Of course, $\Delta x$ and $\Delta t$ are generally linearly related owing to numerical stability and efficiency considerations; the result is only first-order convergence as the resolution is increased. To show that this is not as bad as it might appear, and to compare the new "c" grid schemes with the standard Arakawa "c" grid scheme, we consider the following simple linear problem, forced by a specified bell-shaped pressure field whose amplitude varies with time (see Fig. 1).

The pressure field is designed such that both pressure and its normal derivative vanish on the rectangular boundary of the problem domain. The time dependence is a short-term, early exponential increase, multiplied by a cosine function with a period of 10 days. This is the simplest problem that can address the numerical dispersion effects of various numerical treatments using "c" grid Coriolis terms. Such dispersion is the main disadvantage of the "c" grid. The mathematical statement of the problem can be given as follows:

$$\begin{aligned} \partial u/\partial t &= f v - \Delta p/\Delta x \\ \partial v/\partial t &= -fu - \Delta p/\Delta y \end{aligned} \tag{1}$$

in the rectangular domain $(-\mathrm{LX} < x < \mathrm{LX})$, $(-\mathrm{LY} < y < \mathrm{LY})$. The pressure $p$ is

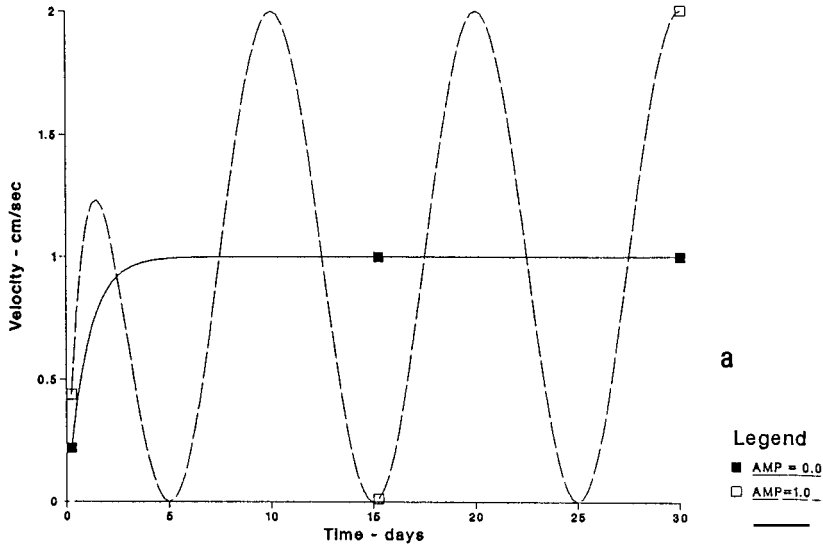


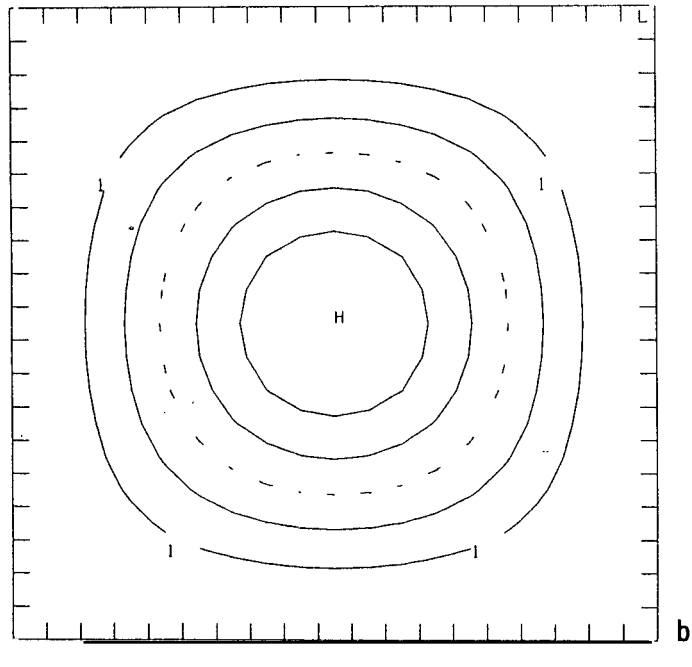


Fig. 1 Specified pressure, $p(x, y, t) = a(t)P(x, y)$. (a) Time dependence, $a(t)$; and (b) spatial structure, $P(x, y)$.

normalized by density, and is specified by

$$p(x, y, t) = A(t)P(x, y)$$

where

$$A(t) = 100[1 - e^{-t/\tau_1}][1 + \text{AMPcos}(2\pi t/\tau_2)] \quad \text{dynes/cm-cm}$$

$$P(x, y) = [(\text{LX} - x)(\text{LY} - y)(\text{LX} + x)(\text{LY} + y)/(\text{LXLY})]$$

The initial conditions are $u = v = 0$. The pressure gradient is evaluated analytically at each grid point at the start of each time step.

The analytic solution to the above system has $u = v = 0$ on the rectangular boundary defined by the four lines $x = \text{LX}$, $y = \text{LY}$, $x = -\text{LX}$ and $y = -\text{LY}$. These conditions are used numerically in all "c" grid results.

Although an analytic solution to the coupled system (1) could be written, it is not of interest here. Our purpose is to compare the errors introduced by the various Arakawa "c" grid interpolation schemes. To do this, we compare the various "c" grid approximate solutions with the *numerical time-differenced solution* of the system (1) on a collocated grid, *using the same time integration scheme*, rather than with the analytic solution. This *numerical time-differenced solution* is derived using analytic derivatives of the specified pressure at the discrete grid points, as the "c" grid solutions are. The collocated grid solution can be called the "analytic solution of the time-differenced system", since no spatial averaging is carried out. The difference between the "c" grid solution and the analytic solution of the time-differenced equations is then due *only* to the errors introduced by the spatial interpolation scheme (see Table 1 caption). The errors are thus not directly affected by the time-difference scheme used.

Conventional "c" grid staggering is used in all "c" grid results. (The outermost pressure points are one-half grid interval inside the boundary. The outermost normal velocity points are on the boundary and the nearest tangential components are one-half grid interval inside.)

Table 1 shows results for 30-day integrations: in all runs $f = 8.342 \times 10^{-5}$ s$^{-1}$, $\tau_1 = 1$ day, $\tau_2 = 10$ days, AMP = 1, and LX = LY = 1000 km. This gives a peak geostrophic velocity of about 2.87 cm s$^{-1}$ after the early transient.

All Table 1 runs use the FLTW time integration scheme (Roache and Dietrich, 1988), with FLT = 0.2. This scheme is a time-filtered leap-frog scheme. At the end of each time step, there are three known time levels of data. The initial value for the next time step is calculated from the three values. If $p_1$, $p_2$ and $p_3$ are the successive values, the initial value, $p$, for the next time step is calculated as follows:

$$p = (1 - \text{FLT})p_2 + \text{FLT}(p_1 + p_3)/2$$

where $0 \leq \text{FLT} \leq 1$.

Here, $p$ for the next time step corresponds to $p_1$ for the present step. This reduces to the leap-frog scheme when FLT = 0. When FLT > 0, selective (high-frequency) time damping results. In the present case, this damps inertial oscillations, but hardly affects the response to the 10-day time-scale shown in Fig. 1. This damping is

analogous to internal wave effects associated with terms not included in the model problem.

Table 1 compares time-average spatial rms errors for the various schemes with spatial resolutions of 12, 24 and 48 grid intervals (in both directions) and with time steps of 45, 90 and 180 min. These "errors" are actually deviations of the "c" grid velocities, interpolated to the cell centres, from the "exact" velocities calculated on a collocated grid. The latter are truly exact solutions to the time-differenced equations, since no spatial interpolations are involved. Since the same time integration schemes, and time step sizes, are used in the comparison with the "c" grid results, it follows that the exact results differ from the "c" grid results only because of spatial truncation errors associated with "c" grid interpolations. The rms errors are thus a direct measure of the accuracy of the various "c" grid schemes. Again, we note that the errors are not directly affected by the time integration schemes; they are only due to spatial interpolations.

The standard base scheme in Table 1 is the Arakawa "c" grid scheme that is popular among "c" grid modellers, in which the $v$ velocity components are interpolated to the $u$ points in evaluating the Coriolis term and vice versa. The new schemes (1A, 1B, 2A and 2B) are described in Section 2 and by DRM.

Table 1 compares the new higher-order Coriolis schemes with their lower-order counterparts and with the standard "c" grid scheme for typical space and time resolutions. The results show that the higher-order schemes are much more accurate. This greatly improved accuracy with relatively low overhead (only a few operations per grid point per time step) shows that the new higher-order schemes are substantial improvements. Similar accuracy improvement could be obtained by using higher-order treatment of the base scheme.

Table 1 also shows that, for a fixed resolution, the errors actually increase with decreasing time step. This is due to the extra interpolations, as noted by DRM. However, since time-step decrease is generally associated with spatial resolution increase, the relevant convergence rate comparison is found by going diagonally downward toward the right in Table 1, or by comparing results for equal spatial resolution and time step. In either case, the higher-order schemes are clearly more accurate, whereas the lower-order schemes are competitive with one another.

Although schemes 2A and 2B appear better than schemes 1A and 1B, we have found that the latter schemes allow longer time steps. Scheme 1B might be the best overall scheme, because longer time steps also mean fewer dispersive interpolations.

Figure 2 shows solution and error plots as a function of time and position along

---

Fig. 2 Mid-latitude ($y = 0$) $x$–$t$ flow speed (a, b) and speed error (velocity error magnitude; c, d). (a) Exact solution for FLT = 0.2; maximum is 4.73 cm $s^{-1}$. At 60 days, the maximum is 2.8687 cm $s^{-1}$. (b) Exact solution for FLT = 1.0; maximum is 3.99 cm $s^{-1}$. At 60 days, the maximum is 2.8696 cm $s^{-1}$. (c) Scheme 1B error for FLT = 0.2; maximum is 0.0022 cm $s^{-1}$. The time-averaged rms error is 0.00069 cm $s^{-1}$. (d) Scheme 1B error for FLT = 1.0; maximum is 0.00063 cm $s^{-1}$. The time-averaged rms error is 0.00020 cm $s^{-1}$. The contours (a) and (b) are uniformly spaced with interval 0.5 cm $s^{-1}$ so that contour level 5 is 2.5 cm $s^{-1}$. Plots (c) and (d) are differences between the (a) and (b) exact solutions and those derived using scheme 1B for the Coriolis terms on a staggered Arakawa "c" grid. The error contours are uniformly spaced between 0 and the maxima specified above.

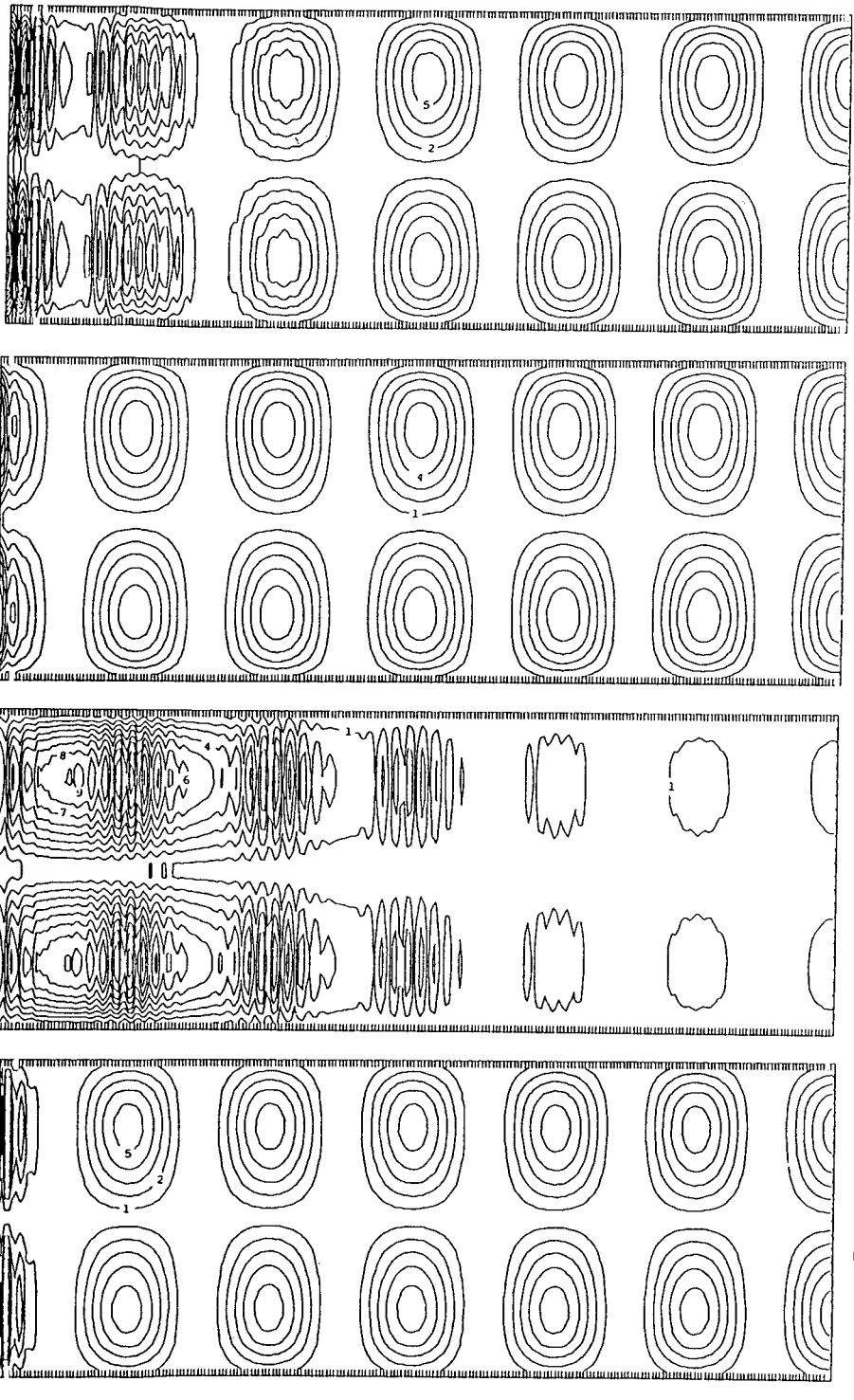
(a)
(b)
(c)
(d)
0 days
60 days

the line $y = 0$ in the problem formulation (1). This line is similar to other lines because of the symmetries and linearity of the problem. The resolution is 24 × 24 and the time step is 90 min. The runs are 60 days. All other parameters are as in the Table 1 runs, except $\tau_1 = 0.1$ day, which triggers a stronger inertial oscillation.

Plots 2a and b show the exact solution to the time-differenced equations for FLT = 0.2 (as in the Table 1 runs) and FLT = 1. These show early inertial oscillations, whose decay leads to the periodic quasi-geostrophic solution forced by the specified time-varying pressure gradient. Using FLT = 1.0 leads to more rapid decay of the high-frequency intertial oscillations, but has little effect on the long-term quasi-geostrophic flow. The difference between the two solutions at 60 days is less than 0.001 cm $s^{-1}$; during the first few inertial periods, it is as large as 0.7 cm $s^{-1}$. This shows that FLT = 1 quickly damps the inertial oscillation, while having an extremely small effect on the response to the 10-day pressure oscillation.

Plots 2c and d show the difference between the scheme 1B numerical solution and these exact solutions, using the same FLT values. The time-averaged rms errors, corresponding to those in Table 1, for FLT = 0.2 and FLT = 1 are 6.9 × and 2.0 × $10^{-4}$ cm $s^{-1}$, respectively. The respective maximum error values of 2.18 × $10^{-3}$ and 6.3 × $10^{-4}$ cm $s^{-1}$ occur during the early transient. The early high-frequency error oscillations reflect errors in representing the rapidly varying transient free inertial oscillation. The much smaller low-frequency error oscillations reflect much smaller errors in the response to the more slowly varying 10-day pressure forcing oscillation.

Thus, Fig. 2 shows that while the inertial oscillations decay due to the time filter (which is similar in effect to internal gravity wave effects that are not included in this problem), the solution approaches a quasi-geostrophic balance with a much smaller error. This clearly shows that the new schemes are more accurate for quasi-geostrophic geophysical modes than for transient inertial oscillations. The latter are relatively unimportant in general circulation calculations as noted in Section 2. As also noted in Section 2, such quasi-geostrophic modes would not be included in initial value problems that address only the Coriolis terms. Thus, analyses of such problems have little relevance to the application of these new schemes to quasi-geostrophic flows.

## 4 Concluding remarks

The Table 1 results clearly demonstrate that the higher-order Coriolis term treatments on an Arakawa "c" staggered grid greatly improve accuracy for low Rossby number flows. Similar improvements would result from treating other large linear terms with higher order for both the "c" and "b" grids. This could approach the accuracy of spectral methods without the associated computational cost and limitations. The potential payoff is much larger than could be achieved by more accurate treatment of the momentum advection terms. The present improvements come with relatively little computational cost, because of the simplicity of the Coriolis terms.

Carrying this philosophy a bit further, one might also consider a more accurate treatment of the vertical density advection term, because of its direct effect on the important Rossby radius of deformation, as Dietrich and Lin have done (1993).

Although horizontal advection is also important, the vertical advection term is generally associated with faster internal wave time-scales and thus might justify more careful treatment.

The $O((\Delta x)^2/\Delta t)$ truncation errors noted by DRM affect mainly the relatively small non-geostrophic (more generally, out-of-balance) part of the flow. However, errors still remain in the steady and slowly varying quasi-geostrophic flow components owing to the Coriolis term interpolations, but all errors are greatly reduced by using higher-order interpolations, as clearly demonstrated by Table 1.

**Acknowledgements**

I would like to acknowledge stimulating discussions with Tom Warn and Charles Lin (McGill University), Bill Simmons (consultant), Eduard Zuur (Groupe Prosper, University of Neuchatel, Switzerland) and John Wormeck (Ecodynamics), and many useful suggestions by the reviewers. This work was supported by grants from the Natural Sciences and Engineering Research Council of Canada and the Department of Fisheries and Oceans.

## Appendix 1: The new "c" grid Coriolis schemes

Here, we describe the new schemes 1A and 1B in detail as in DRM. For additional discussion, and a detailed description of schemes 2A and 2B, see DRM.

We describe these schemes with reference to simplified equations. Since the distinguishing features of the methods concern only the time derivative terms, the Coriolis terms and the vertical diffusion terms of the momentum equations, the remaining terms are lumped into $U$ and $V$, and the simplified momentum equations are

$$\begin{aligned} \frac{\partial u}{\partial t} &= U + fv + uz \\ \frac{\partial v}{\partial t} &= V - fu + vz \end{aligned} \tag{A-1}$$

where $uz$ and $vz$ are the vertical diffusion terms and $f$ is the Coriolis parameter in the Coriolis acceleration terms, which varies only with latitude. In the model problem of the main text, $U$ and $V$ contain only the pressure gradient, and $uz$ and $vz$ are zero.

**a** *Scheme 1A*

This is the SOMS algorithm described by Dietrich et al. (1987). The procedure is as follows:

1) Calculate the $U(i,j,k)$ and $V(i,j,k)$ terms in the following schematic representation of the staggered "c" grid control volume equations:

$$\begin{aligned} u(i+\tfrac{1}{2},j,k,n+1) &= u(i+\tfrac{1}{2},j,k,n) + \Delta t[U(i+\tfrac{1}{2},j,k) + fv + uz] \\ v(i,j+\tfrac{1}{2},k,n+1) &= v(i,j+\tfrac{1}{2},k,n) + \Delta t[V(i,j+\tfrac{1}{2},k) - fu + vz] \end{aligned} \tag{A-2}$$

The $U$ and $V$ terms are integrated explicitly (in time).

2) Interpolate the explicit terms $U$ and $V$, and the old time level $u$ and $v$ velocity components to the $p$ locations, using simple two-point centred averages:

$$\begin{aligned} U(i,j,k) &= [U(i+1/2,j,k) + U(i-1/2,j,k)]/2 \\ V(i,j,k) &= [V(i,j+1/2,k) + V(i,j-1/2,k)]/2 \\ u(i,j,k,n) &= [u(i+1/2,j,k,n) + u(i-1/2,j,k,n)]/2 \\ v(i,j,k,n) &= [v(i,j+1/2,k,n) + v(i,j-1/2,k,n)]/2 \end{aligned} \tag{A-3}$$

3) Integrate the full equations, including the implicitly coupled Coriolis and vertical diffusion terms at the $p$ locations:

$$\begin{aligned} u(i,j,k,n+1) &= u(i,j,k,n) \\ &\quad + \Delta t[U(i,j,k) + f v(i,j,k,n+1) + uz(i,j,k,n+1)] \\ v(i,j,k,n+1) &= v(i,j,k,n) \\ &\quad + \Delta t[V(i,j,k) - fu(i,j,k,n+1) + vz(i,j,k,n+1)] \end{aligned} \tag{A-4}$$

4) Interpolate the results from step (3) back to the staggered $u$ and $v$ locations:

$$\begin{aligned} u(i+1/2,j,k,n+1) &= [u(i,j,k,n+1) + u(i+1,j,k,n+1)]/2 \\ v(i,j+1/2,k,n+1) &= [v(i,j,k,n+1) + v(i,j+1,k,n+1)]/2 \end{aligned} \tag{A-5}$$

5) Clear out the divergence of the barotropic mode (vertically averaged horizontal flow) by solving a two-dimensional Poisson equation for the surface pressure correction "*dp*" (see Dietrich et al., 1987); correcting the pressure gradient in the $U$ and $V$ terms in (A-1); and adding the effects of the corrected pressure gradient (the correction is independent of depth) everywhere to the new $u$ and $v$ velocity components:

$$\begin{aligned} u(i+1/2,j,k,n+1) &= u(i+1/2,j,k,n+1) + \Delta t[dp(i+1,j) - dp(i,j)] \\ v(i,j+1/2,k,n+1) &= v(i,j+1/2,k,n+1) + \Delta t[dp(i,j+1) - dp(i,j)] \end{aligned} \tag{A-6}$$

This adjustment is performed explicitly, without implicit coupling to Coriolis terms.

6) Calculate the vertical velocity by integrating the incompressibility equation.

7) Apply the "filtered leapfrog" updating scheme described in Section 3 to start the next time step.

**b** *Scheme 1B*

Scheme 1B is like scheme 1A except the interpolations between the $p$ locations and the "c" grid staggered $u$ and $v$ locations are performed with higher accuracy. In particular, instead of interpolating the two nearest locations to the central point, a cubic is fit through four nearby locations, and the result is evaluated at the central location. For example, let four successive $u$ values along a latitude be $u(i), i = 1,4$. Then, the original, lower-order interpolation scheme used in scheme 1A is given by

$$u(i+1/2) = [u(i) + u(i+1)]/2 \tag{A-7}$$

and the new higher-order interpolation used in scheme 1B is

$$u(i + 1/2) = \{9[u(i) + u(i + 1)] - [u(i - 1) + u(i + 2)]\}/16 \qquad \text{(A-8)}$$

## References


ARAKAWA, A. and V.R. LAMB. 1981. A potential enstrophy and energy conserving scheme for the shallow water equations. *Mon. Weather Rev.* **109**: 18–36.

BATTEEN, M.L. and R.J. HAN. 1981. On the computational noise of finite-difference schemes used in ocean models. *Tellus*, **33**: 387–396.

BRYAN, K. and M.D. COX. 1968. A nonlinear model of an ocean driven by wind and differential heating: Parts I and II. *J. Atmos. Sci.* **25**: 945–978.

COX, M.D. 1984. A primitive equation three-dimensional model of the ocean. Tech. Rep. 1, Geophys. Fluid Dyn. Lab., NOAA, Princeton, N.J., 250 pp.

DAVIES, A.M. and G.K. FURNES. 1980. Observed and computed M2 tidal currents in the North Sea. *J. Phys. Oceanogr.* **16**: 237–257.

DIETRICH, D.E. 1972. A numerical study of rotating baroclinic flows in the rotating annulus experiments. Ph.D. Thesis, Florida State University, Tallahassee, Fla., 131 pp.

——— and N. BRUNET. 1979. Precipitation modulation by large-scale inertia-gravity waves. *J. Meteorol. Soc. JPN*, **57**: 469–473.

——— and D.-S. KO. 1993. Shelf resolving numerical studies of the Gulf of Mexico. *J. Geophys. Res.* in print.

——— and C.A. LIN. 1993. A study of Gulf of Mexico eddy shedding using SOMS. *J. Geophys. Res.*, submitted.

———; M.G. MARIETTA and P.J. ROACHE. 1987. An ocean modeling system with turbulent boundary layers and topography: Numerical description. *Int. J. Numer.* Meth. *Fluids*, **7**: 833–855.

———; P.J. ROACHE and M.G. MARIETTA. 1990. Convergence studies with the Sandia Ocean Modeling System. *Int. J. Numer. Meth. Fluids*, **11**: 127–150.

FOREMAN, M.G.G. 1987. An accuracy analysis of selected finite difference methods for shelf waves. *Cont. Shelf Res.* **7**: 773–803.

MELLOR, G.L. and T. YAMADA. 1982. Development of a turbulence closure model for geophysical fluid problems. *Rev. Geophys. Space Phys.* **30**: 851–875.

MESSINGER, F. and A. ARAKAWA. 1967. Numerical methods used in atmospheric models. GARP Publ. Ser. No. 17, Vol. 1, World Meteorological Organization, Geneva, Switzerland.

ROACHE, P.J. and D.E. DIETRICH. 1988. Evaluation of the leapfrog-trapezoidal time integration method. *Numer. Heat Transfer*, **14**: 149–164.

WAJSOWICZ, R.C. 1986a. Free planetary waves in finite-difference numerical models. *J. Phys. Oceanogr.* **16**: 773–789.

——— 1986b. Adjustment of the ocean under buoyancy forces. Part II: The role of planetary waves. *J. Phys. Oceanogr.* **16**: 2115–2136.

——— and A. GILL. 1986. Adjustment of the ocean under buoyancy forces. Part I: The role of Kelvin waves. *J. Phys. Oceanogr.* **16**: 2097–2114.

ZUUR, E.A.H. and D.E. DIETRICH. 1990. The SOMS model and its application to Lake Neuchatel. *Aquat. Sci.* **52**: 115–129.